Acta Acustica 2025, **9**, 83

https://doi.org/10.1051/aacus/2025066

Available online at:
https://acta-acustica.edpsciences.org

SCIENTIFIC ARTICLE OPEN ACCESS

# Experimental study of acoustic streaming in microchannels generated by pulsed focused ultrasound

Elisa Ghiringhelli[1,*], Philippe Lasaygues[2], Carine Guivier-Curien[1], and Cécile Baron[1]

[1]Aix Marseille Univ, CNRS, Centrale Méditerranée, IRPHE UMR 7342, Marseille, France
[2]Aix Marseille Univ, CNRS, Centrale Méditerranée, LMA UMR 7031, Marseille, France

Received 18 September 2025, Accepted 21 November 2025

**Abstract** – Pulsed focused ultrasound (p-FUS) are gaining interest across a range of applications, such as regenerative medicine, neurostimulation and targeted drug delivery, offering a non-invasive therapeutic approach. In order to gain insight into the hydrodynamic effects potentially induced by p-FUS in biological tissues, the present acoustofluidic study investigates the ability of focused ultrasound to generate acoustic streaming in a viscous fluid confined in a microchannel. Through micro-particle image velocimetry ($\mu$PIV) measurements, it analyses the flow patterns induced by p-FUS in a rectangular cross-section microchannel, corresponding to half of the ultrasonic wavelength. The analysis confirmed good repeatability across replicates, despite minor variations introduced by manual assembly. It is shown that the flow patterns reach the equilibrium within seconds and that the average streaming velocity varies quadratically with the duty cycle characterizing p-FUS. Moreover, the results indicate that the streaming velocity magnitude depends on the amount of acoustic energy delivered to the channel. Interestingly, the induced flow exhibits a strongly three-dimensional structure, revealing spatial dynamics that, to our knowledge, have not been previously observed in microscale acoustic streaming studies. These results lay the foundation for understanding the interaction of p-FUS with a confined fluid at the microscale, opening new avenues for investigating more complex networks and porous media representing biological tissues.

**Keywords.** Focused ultrasounds, Acoustic streaming, Acoustofluidics

## 1 Introduction

Pulsed focused ultrasound (p-FUS) therapies have emerged as a promising non-invasive modality for various medical applications, including enhancing tissue regeneration and healing [1], facilitating neurostimulation [2], and improving drug delivery [3]. p-FUS are particularly effective due to its ability to propagate through biological media and concentrate acoustic energy at a focal point, enabling precise interaction with micrometric channel networks found in tissues such as the microvasculature [4], bone lacuno-canalicular network [5], and lymphatic system [6]. Despite their growing use and encouraging outcomes, the fundamental mechanisms underlying their therapeutic effects remain poorly understood. We hypothesize that acoustic streaming potentially generated by p-FUS within a confined fluidic cellular microenvironment plays a key role in mediating these effects. However, to our knowledge, p-FUS have yet to be studied on controlled benchmark models. To address this gap, our goal is to investigate the interaction between p-FUS and fluid-filled microchannels.

Acoustofluidics, a field that integrates ultrasound waves with microfluidic systems, has emerged as a transformative technology in manipulating particles and fluids [7]. In this context, two primary main mechanisms govern particle and fluid motion: acoustic radiation forces [8] and acoustic streaming [9]. The acoustic radiation force arises from interactions between microparticles in a fluid and ultrasound waves, as it results from momentum transfer due to pressure gradients in the wave field, acting directly on particles depending on their size and their acoustic contrast with the surrounding fluid [10]. Acoustic streaming refers to the steady fluid motion that results from the absorption of acoustic energy by the fluid [11]. In microfluidic channels, considering MHz-frequency, acoustic streaming occurs due to thermoviscous effects [12, 13]. Understanding how p-FUS interact with a fluid in microchannels is essential for optimizing p-FUS therapies. The purpose of this study is to highlight the ability of p-FUS to induce acoustic streaming in a fluid confined in microchannels as this phenomenon is likely to be at the

*Corresponding author: elisa.ghiringhelli@univ-amu.fr

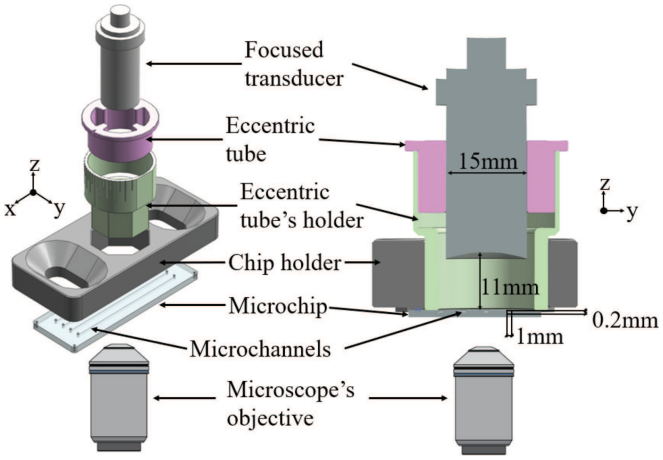


**Figure 1.** Scheme of the experimental set-up. (Left) view of the split components of the assembly; (right) cross-section of the assembly. Dimensions of the channel are not scaled for visualization purposes.

origin of cells response observed in biological tissues [14]. To this end, an experimental study is carried out, where p-FUS are emitted within a fluid microchannel, aiming to identify and characterize the acoustic streaming. In particular, the $\mu$PIV, technique [15, 16] is employed to measure the streaming velocity field ($v$) in a rectangular cross-sectional microchannel.

## 2 Experimental method

To characterize the fluid flow induced by p-FUS in a microchannel, a custom acousto-microfluidic system was designed and developed to integrate a FUS transducer and a microchip (microfluidic ChipShop, Germany) on an inverted episcopic microscope (Fig. 1), already integrated into a $\mu$PIV platform. The transducer was held in place by an eccentric tube, allowing adjustments on both the axial $z$-direction and lateral $y$-direction of the US focal point with respect to the channel with an accuracy of $\pm 10\,\mu$m. In particular, the alignment of the ultrasound focal point with the channel's center was determined by observing the acoustic streaming flow pattern generated within the channel. The pattern is known to be symmetric with respect to both the $x$ and $y$ axes, allowing precise identification of the channel center for alignment.

The eccentric tube holder (Fig. 1), which was sealed at the bottom with a thin plastic membrane, was filled with deionized water to ensure the propagation of ultrasonic waves from the transducer. The chip and the tube are held in place by a holder to facilitate the alignment between the focal point and the channel.

Experiments were carried out with Poly methyl methacrylate (PMMA) microfluidic chips (microfluidic ChipShop, Germany). The channels were engraved on a 1.5 mm thick PMMA plate sealed with a 175 $\mu$m thick cover lid. A rectangular cross-section microchannel (Fluidic 138), 1000 $\mu$m $\times$ 200 $\mu$m, respectively in the $y$, $z$ directions, referred $C_{1000/200}$, was used. All experiments were carried out in a closed channel, filled with a solution of water and particles.

In order to characterize the flow patterns, microparticle image velocimetry ($\mu$PIV) measurements were performed. To do so, distilled water (DI water) was seeded with 1 $\mu$m diameter carboxylate-modified fluorescent polystyrene microspheres (535/575, FluoSpheres F8819, Invitrogen, France). The particles were excited by a double-pulsed 532 nm laser light (NdYag Gemini PIV, New Wave Research, USA) and imaged with a 12 bit 5.5 Mpixel digital sCMOS camera (Andor Zyla sCMOS, Andor, France) controlled by a synchronizer. The optical plane was placed at mid-height ($z$-direction) of the microchannel and the thickness of the plane was determined from the calculation of the depth of correlation [17], which gave $d_z = 27.58\,\mu$m for the experiments realized with an UPLFLN 10X microscope lens. At such a magnification, the field of view was $1.7 \times 1.44\,\text{mm}^2$ for the full maximum image resolution of $2560 \times 2160\,\text{pixel}^2$. It is noteworthy that all the following $\mu$PIV treatment results are microparticle velocities averaged over $d_z$. Open source software DPIV-Soft 2010 was used for the $\mu$PIV image processing [18].

A spherically focused single element transducer with a center frequency ($-6$ dB) of 5 MHz $\pm 10\%$ (Imasonic, Voray-sur-l'Ognon, France) was used for all experiments. The radius of curvature was 15 mm. The focal spot size at $-3$ dB was 4 mm (focus depth $z$-direction) $\times$ 0.8 mm (spot diameter $xy$-plane). The transducer was driven using a waveform generator (TU-TGF4242, Thurlby Thandar Instruments Limited, UK) coupled with a power amplifier (KMP Electronic, model 44702, 150 W, 0.5–15 MHz, Bulgaria). The frequency ($f$) of the temporal source waveform was chosen to be 3.75 MHz, corresponding to the resonance frequency of 200 $\mu$m width-channels full of water. This configuration generates a standing wave in the microchannel. The driving signal is defined by a duty cycle DC, and its pulse repetition period $T_{\text{PR}}$ in $\mu$s. Each pulse consists of a sequence of sound waves, described by a "on" period $T_{\text{on}}$, followed by a pause $T_{\text{off}}$, before the next pulse is emitted. By defining the pulse repetition period as $T_{\text{PR}} = T_{\text{on}} + T_{\text{off}}$, the duty cycle is $\text{DC} = T_{\text{on}}/T_{\text{PR}}$. In these experiments, $T_{\text{PR}} = 100\,\mu$s. To further characterize the ultrasound stimulation, Spatial Average Time Average Intensity $I_{\text{SATA}}$ is defined as a linear function of DC:

$$I_{\text{SATA}} = \frac{\langle p^2 \rangle}{Z} \times \text{DC} \tag{1}$$

where $\langle . \rangle$ is the time average operator, $p$ is the acoustic pressure and $Z$ the acoustic impedance.

The acoustic pressure is driven by the peak-to-peak voltage $V_{pp} = 113$ mV for the continuous signal (DC = 1). It can be modified to maintain $I_{\text{SATA}}$ constant, while changing DC.

## 3 Results and discussion

This article explores the effect of p-FUS applied to a microchannel filled with water. First we prove the repeatability of the experiments by introducing a similarity index. Then, several outcomes are reported, on the DC's influence on the flow velocity along with the impact of the channel's size. In the mid-height of the channel, a four quadrant, steady acoustic streaming pattern symmetric to the center of the channel was formed, Figures 2a and 2b. Here, the streaming velocity is measured via the $\mu$PIV treatment. Indeed, the particles' diameter is sufficiently small to ensure that the effect of the radiation force is negligible. Furthermore, experiments are stopped after 6 s, as longer periods saw an accumulation of particles at the vortexes' centers. This phenomenon was previously proven, revealing that even with small particles, a weak component of radiation force still acts on them, forming depletion regions at late times [19].

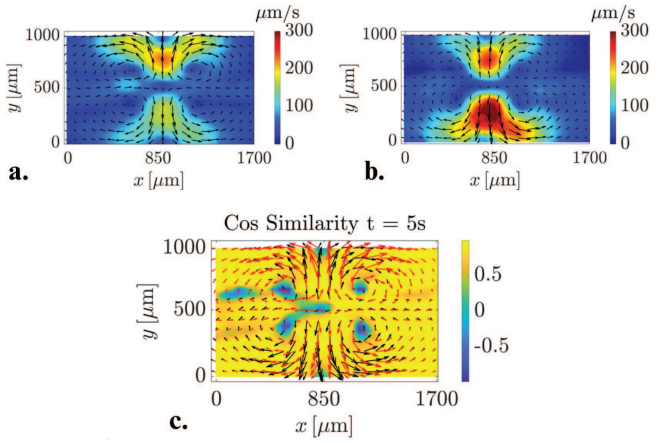


**Figure 2.** (a) and (b) Velocity fields, obtained from PIV treatment, of two experiments in a continuous configuration for $C_{1000/200}$ at the same time step $t = 5$ s where the color map represents the velocity amplitude. (c) The relative $S_c$ distribution with the velocity field.

### 3.1 Repeatability

To demonstrate the repeatability of the experiments, the *cosine similarity* is introduced. It is a measure of similarity between two non-zero vectors defined in an inner product space. Considering two 2-dimensional vectors, $\mathbf{a}(x, y)$ and $\mathbf{b}(x, y)$, the cosine similarity $S_C(x, y)$ is defined as the cosine of the angle $\theta$ between them:

$$S_C(x, y) = \frac{\mathbf{ab}}{|\mathbf{a}||\mathbf{b}|} = \cos\theta \tag{2}$$

therefore $S_C \in [-1, 1]$.

This index is computed for each couple of vectors in the same position $(x, y)$ of two velocity fields.

As shown in Figures 2a and 2b, at the same time step ($t = 5$ s), the four-rolls patterns look similar for two different experiments carried out with the same parameter sets even though the streaming velocity magnitude is differently distributed. However, the cosine similarity map in Figure 2c, reveals that the direction of the velocity vectors has an overall agreement of 80%. The most important difference is the alignment of the vortexes centers, where the vectors are associated to low velocities and an error can be introduced from the $\mu$PIV processing of the images. In fact, the upper vortexes of Figure 2a are slightly shifted upward, $y = 650\,\mu$m, while in Figure 2b, they are centered at $y = 700\,\mu$m, the same shift is observed for those in the bottom region. This difference in position is clearly visible in Figure 2c, where the velocity fields of both experiments are superimposed. Overall, as the system is set up manually, a slight offset in transducer positioning cannot be ruled out, and it may result in a considerable difference in streaming velocity distribution and a slight alteration in field directionality.

### 3.2 Tuning of DC and wave amplitude

This section shows how the tuning of the duty cycle and of the wave amplitude affect the streaming velocity. By keeping the signal amplitude constant to $V_{pp} = 113$ mV, the $I_{\mathrm{SATA}}$ changes as a function of the duty cycle. This value of $V_{pp}$ was chosen first to accommodate the limitations of the imaging system with a maximum acquisition frequency of 15 Hz, since, as signal amplitude increases, so does the particles' velocity [20]. Secondly, it prevents thermal effects that could damage the PMMA cover lid [21].

Figure 3a shows the average streaming velocities in time for different values of DC. From the PIV results, the average velocity was obtained by spatially averaging all velocity vectors within the field of view. The study reveals two key findings, first, the velocity reaches a plateau value that increases with DC, and second, the transient period to reach the equilibrium is longer as DC increases. This phenomenon can be explained by temperature gradients in the medium, which increase with the acoustic energy over time and cannot be neglected in the context of low-intensity p-FUS in a microchannel. As DC decreases, the temperature gradients become less intense, resulting in shorter transition times (Fig. 3a), which means that the thermoacoustic streaming approaches Rayleigh streaming where there are no temperature gradients [13]. This interpretation should be considered preliminary until confirmed by future experimental validation.

The dependence of the average velocity on DC is investigated for a given value of $\mathrm{I_{SATA}}$. This value is chosen to correspond to the intensity of the continuous configuration (DC = 1) obtained for $V_{pp} = 113$ mV. Referring to equation (1), $\mathrm{I_{SATA}}$ is quadratically dependent on the acoustic peak pressure, which is proportional to the amplitude of the signal, $A_{\mathrm{DC}}$. Consequently, to maintain

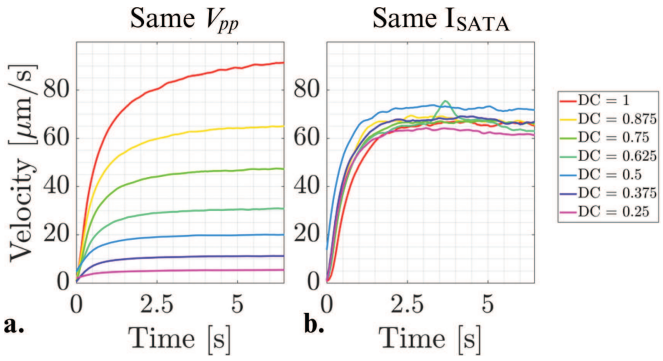


**Figure 3.** Evolution of the average velocities in time for different duty cycles: (a) the voltage $V_{pp} = 113\,\text{mV}$ remains constant, while $I_{SATA}$ changes with DC. (b) $I_{SATA}$ is maintained constant by adjusting $V_{pp}$ for every duty cycle.

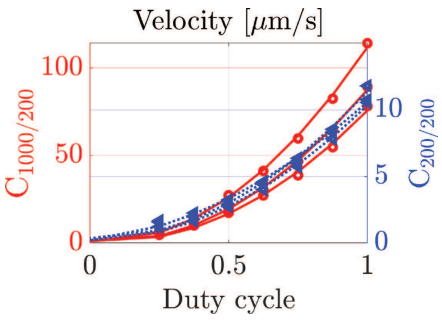


**Figure 4.** Average velocities for a defined time step $t = 5\,\text{s}$, the lines represent the quadratic fitting of the data. Each group of three lines in the red and blue curves corresponds to independent repetitions of the same experimental condition. This approach highlights the reproducibility of the measurements and the reliability of the observed trends.

the same $I_{SATA}$, $A_{DC}$ should be adapted as:

$$A_{DC} = A_1/\sqrt{DC} \tag{3}$$

where $A_1 = V_{pp} = 113\,\text{mV}$. Figure 3b shows the evolution of the average velocities. As expected, stimulating the fluid with the same acoustic intensity, results in a fluid flow alike whatever DC. The mean equilibrium velocity reached by the flow is measured to be $67\,\mu\text{m/s} \pm 7\,\mu\text{m/s}$. Notice that the experiments related to Figures 3a and 3b, were not conducted during the same run, otherwise the equilibrium values for DC = 1 would have been approximately equal.

### 3.3 Dependence on the channel size

The average velocities, obtained from three different experiments with the same amplitude in $C_{1000/200}$ at a fixed time step $t = 5\,\text{s}$, are plotted as a function of DC in Figure 4. To complement the study, experiments are carried out in a smaller channel with squared section $200\,\mu\text{m} \times 200\,\mu\text{m}$ ($C_{200/200}$)n see Figure 4. At this moment, the steady state is reached for every DC. The average velocity value for DC = 0, is imposed to be zero. It can be observed that when the flow is in equilibrium, the average velocity becomes proportional to $DC^2$, therefore $v \propto {I_{SATA}}^2$, from equation (1). Notice that, in Figure 4, there is a difference of about $25\,\mu\text{m/s}$ from one experiment to the other for the continuous case (DC = 1), in $C_{1000/200}$. The reason is likely to be transducer positioning in relation to the channel, since it is done manually. Even if the velocities in $C_{200/200}$ reach a maximum of $10\,\mu\text{m/s}$, the parabolic trend is equal to $C_{1000/200}$.

In $C_{1000/200}$, particles reach an average velocity of $\approx 100\,\mu\text{m/s}$ (Fig. 4), while in $C_{200/200}$, the maximum velocity is reduced by an order of magnitude. This decrease in velocity magnitude could be attributed on the one hand, to more significant boundary effects in $C_{200/200}$, and, on the other hand, possibly to the size of the focal zone of the acoustic field relative to the channel's dimensions. Indeed, for $C_{1000/200}$, the integrality of the $800\,\mu\text{m}$ diameter focal spot is contained inside the microchannel. This means that all the acoustic power $W_{1000/200}$ is delivered to the fluid through a surface $A_{1000/200} = 16 \cdot 10^4 \pi \mu\text{m}^2$. However, in $C_{200/200}$, the focal spot overflows the microchannel and the sonicated area is reduced to $A_{200/200} = 16 \cdot 10^4\,\mu\text{m}^2$. As the acoustic power is proportional to this surface (for a given $V_{pp}$) [22], it means that $W_{200/200} = W_{1000/200}/\pi$. Finally, assuming that the acoustic field amplitude is small enough to consider the streaming velocity $v$ proportional to $(W^2)$ [23], then $v_{1000/200} = \pi^2 v_{200/200} \approx 10 v_{200/200}$ which corresponds to the ratio estimated from Figure 4.

### 3.4 Three-dimensional flow

In the literature, when ultrasound are applied to a microchannel filled with water, different flow structures are generated depending on the dimensions of the microchannel, the frequency and so on. These structures are found to be two-dimensional in the cross-section of the channel [24];

To compare these results with our experiments, the patterns and the velocity magnitude of the flow are plotted for three positions of the optical focal plane in $C_{1000/200}$ at $t = 2\,\text{s}$ (Fig. 5). This provides evidence of the complexity and the three-dimensionality of the flow induced by p-FUS in terms of changes in flow direction and velocity magnitude distribution.

Close to the bottom of the channel ($33\,\mu\text{m}$) or to the top ($166\,\mu\text{m}$), the flow patters and magnitudes differ significantly from the four vortexes formed at $100\,\mu\text{m}$. This mismatch on different planes suggests the presence of recirculations in the $z$ direction. However, the current experimental set up is technically unable to measure the three-dimensional flow, reason why the previous analyses were carried out in the $z$-middle plane only, corresponding to the location of the pressure node created in the microchannel.

These experimental observations, although obtained under simplified laboratory conditions, provide insight

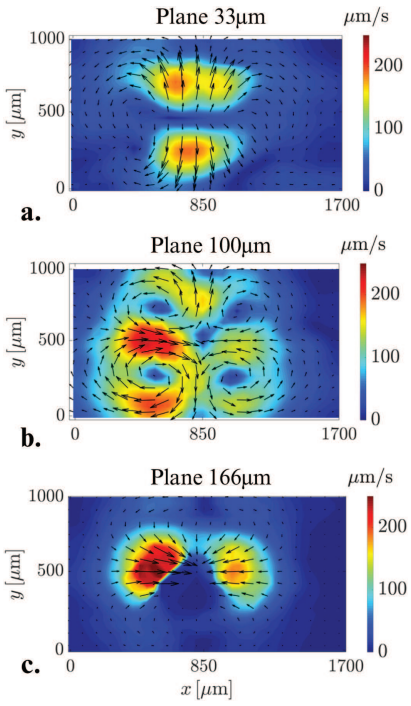


**Figure 5.** Velocity field obtained from $\mu$PIV image treatment at a given time $t = 2\,\mathrm{s}$, for different optical focal planes (a) $z = 33\,\mu\mathrm{m}$, (b) $z = 100\,\mu\mathrm{m}$ and (c) $z = 166\,\mu\mathrm{m}$ from the bottom of the channel.

into mechanisms that may occur in biological microenvironments exposed to pulsed focused ultrasound. In particular, the formation of steady and three-dimensional acoustic streaming patterns in confined geometries supports the hypothesis that similar hydrodynamic effects could act as mechanical stimuli within tissue-scale microvascular or lacuno-canalicular networks. In biological systems, however, the geometries are far more complex and irregular, which would significantly affect both the streaming patterns and the optimal excitation frequency. Identifying the effective acoustic parameters in such heterogeneous environments would require combined experimental and numerical approaches, built on the understanding established by this simplified model.

## 4 Conclusion

This article lays the groundwork to investigate the effects of p-FUS in microchannels. A $\mu$PIV image processing has been applied to study the patterns and magnitude of the streaming velocities in a 2D $xy$ plane. We demonstrated the repeatability of the experiments by introducing cosine similarity analysis, which confirmed that the overall trends are consistent across replicates, while allowing minor variations resulting from manually assembled systems. We showed that maintaining a constant $V_{pp}$ for every duty cycle, results in a lower equilibrium velocity and a shorter transient period as DC decreases. These results reflect a transition from thermoacoustic streaming to boundary-driven one. Although the influence of temperature was not explored, it is intended to be examined in future work along with appropriate numerical simulations. Further, we compared the streaming in channels of different sizes, finding that variations in the velocity depend on how much of the focal spot is confined within the channel. Finally, by changing the optical plane, it emerged that the fluid flow exhibits a pronounced three-dimensional complexity, in clear contrast to the predominantly two-dimensional character reported in the existing literature. This finding reveals the need for a deeper investigation of the flow's full spatial structure. To this end, future work will focus on modifying the platform to enable wider analysis of these three-dimensional flow features. Although experimental in nature, this study serves as a preliminary exploration for a better understanding of the interaction of pulsed focused ultrasound with fluids and particles confined in a micro-geometry.

### Acknowledgments

The authors would like to thank Eric Bertrand for his help in developing the experimental set-up and Wei Qiu for the insightful discussions.

### Funding

The project leading to this publication has received funding from the Excellence Initiative of Aix-Marseille University – A*Midex, a French "Investissements d'Avenir programme" – Institut Mécanique et Ingénierie (IMI, AMX-19-IET-010), and the French National Research Agency (ANR), under grant ANR-22-CE51-0038-01 (INVICT-US project).

### Data availability statement

The research data associated with this article are available in Amubox, under the reference https://amubox.univ-amu.fr/s/5YBJc6LcmMgJN4W.

### References

1. B. de Lucas, L.M. Pérez, A. Bernal, B.G. Gálvez: Ultrasound therapy: experiences and perspectives for regenerative medicine. Genes (Basel) 11, 9 (2020) 1086.
2. H.A.S. Kamimura, A. Conti, N. Toschi, E.E. Konofagou: Ultrasound neuromodulation: mechanisms and the potential of multimodal stimulation for neuronal function assessment. Frontiers in Physics 8 (2020) 150.
3. H.-D. Liang, J. Tang, M Halliwell: Sonoporation, drug delivery, and gene therapy. Proceedings of the Institution of Mechanical Engineers, Part H: Journal of Engineering in Medicine 224, 2 (2010) 343–361.
4. F. Mohamad Yusoff, M. Kajikawa, T. Sakamoto, A. Tanaka, Y. Higashi: Low-intensity pulsed ultrasound for "no-option" chronic/critical limb-threatening ischaemia in a patient with Buerger disease: a case report. European Heart Journal – Case Reports 8, 6 (2024) ytae246.
5. S. Schandelmaier, A. Kaushal, L. Lytvyn, D. Heels-Ansdell, R.A.C. Siemieniuk, T. Agoritsas, G.H. Guyatt, P.O. Vandvik, R. Couban, B. Mollon, J.W. Busse: Low intensity pulsed ultrasound for bone healing: systematic review of randomized controlled trials. BMJ 356 (2017) j656.

6. Z. Liu, J. Li, Y. Bian, X. Zhang, C. Xiaojun, Y. Zheng: Low-intensity pulsed ultrasound reduces lymphedema by regulating macrophage polarization and enhancing microcirculation. Frontiers in Bioengineering and Biotechnology 11 (2023) 1173169.
7. B. Cha, S.H. Lee, S.A. Iqrar, H.-G. Yi, J. Kim, J. Park: Rapid acoustofluidic mixing by ultrasonic surface acoustic wave-induced acoustic streaming flow. Ultrasonics Sonochemistry 99 (2023) 106575.
8. A. Doinikov: Acoustic radiation force on a spherical particle in a viscous heat-conducting fluid. III. Force on a liquid drop. The Journal of the Acoustical Society of America 101 (1997) 731–740.
9. W.L. Nyborg: Acoustic streaming near a boundary. The Journal of the Acoustical Society of America 30, 4 (1958) 329–339.
10. H. Bruus: Acoustofluidics 7: the acoustic radiation force on small particles. Lab on a Chip 12, 6 (2012) 1014.
11. W. Qiu, J.T. Karlsen, H. Bruus, P. Augustsson: Experimental characterization of acoustic streaming in gradients of density and compressibility. Physical Review Applied 11, 2 (2019) 024018.
12. J.H. Joergensen, W. Qiu, H. Bruus: Transition from boundary-driven to bulk-driven acoustic streaming due to nonlinear thermoviscous effects at high acoustic energy densities. Physical Review Letters 130, 4 (2023) 044001.
13. W. Qiu, J.H. Joergensen, E. Corato, H. Bruus, P. Augustsson: Fast microscale acoustic streaming driven by a temperature-gradient-induced nondissipative acoustic body force. Physical Review Letters 127, 6 (2021) 064501.
14. X. Guo, M. Sun, Y. Yang, H. Xu, J. Liu, S. He, Y. Wang, L. Xu, W. Pang, X. Duan: Controllable cell deformation using acoustic streaming for membrane permeability modulation. Advanced Science (Weinh) 8, 3 (2021) 2002489.
15. R. Lindken, M. Rossi, S. Große, J. Westerweel: Microparticle image velocimetry ($\mu$PIV): recent developments, applications, and guidelines. Lab on a Chip 9, 17 (2009) 2551.
16. A. Etminan, Y.S. Muzychka, K. Pope, B. Nyantekyi-Kwakye: Flow visualization: state-of-the-art development of micro-particle image velocimetry. Measurement Science and Technology 33, 9 (2022) 092002.
17. S.T. Wereley, C.D. Meinhart: Recent advances in microparticle image velocimetry. Annual Review of Fluid Mechanics 42, 1 (2010) 557–576.
18. P. Meunier, T. Leweke: Analysis and treatment of errors due to high velocity gradients in particle image velocimetry. Experiments in Fluids 35 (2003) 408–421.
19. W. Qiu, H. Bruus, P. Augustsson: Particle-size-dependent acoustophoretic motion and depletion of micro- and nano-particles at long timescales. Physical Review E 102, 1 (2020) 013108.
20. J. Lei, P. Glynne-Jones, M. Hill: Acoustic streaming in the transducer plane in ultrasonic particle manipulation devices. Lab on a Chip 13, 11 (2013) 2133.
21. Y. Long, Y. Gan, F. Sun, Y. Zhao: Study on the heating law of thermal effect of HIFU on tissue based on piezoelectric ceramic voltage and vibration frequency. Scientific Reports 15, 1 (2025) 4168.
22. P. Acevedo and D. Das-Gupta: The measurement of the spatial average temporal average intensity Isata and ultrasonic power $W$ in composite ultrasonic transducers for medical application. Ultrasonics 40, 1 (2002) 819–821.
23. I. Zhvaniya, I. Konopatskaya, M. Mironov, P. Pyatakov: Acoustic streaming exited by focused ultrasound. Acoustical Physics 67 (2021) 245–249.
24. R. Barnkob, P. Augustsson, T. Laurell, H. Bruus: Acoustic radiation- and streaming-induced microparticle velocities determined by microparticle image velocimetry in an ultrasound symmetry plane. Physical Review E 86, 5 (2012) 056307.


**Cite this article as:** Ghiringhelli E. Lasaygues P. Guivier-Curien C. & Baron C. 2025. Experimental study of acoustic streaming in microchannels generated by pulsed focused ultrasound. Acta Acustica, **9**, 83. https://doi.org/10.1051/aacus/2025066.